Microstructural and Mechanical Characterization of AlSi10Mg Additively Manufactured Material Using Direct Metal Laser Sintering Technique

S. P. Tan, M. A. Ramlan, M. S. Shaari, Akiyuki Takahashi, and M. R. M. Akramin

Abstract AlSi10Mg alloy produced by additive manufacturing (AM) technology using direct metal laser sintering (DMLS) technique has resulted better in handling complex geometry. However, limited studies are performed for this AM method to show the integrity of aluminium alloys produced by DMLS to meet the required industry standard. This study investigates the effect of post-process on microstructure, mechanical properties, and fatigue life behaviour to AlSi10Mg material that DMLS produces. In this study, the specimens were tested with different post-process types: annealing (TS) and heat treatment processes (T5 and T6 conditions). All test results were compared with as-built processed specimens. Scanning electron microscope (SEM) and optical microscope are used to capture the microstructure images. The results showed that the tensile strength of the post-processed was decreased approximately 25% (decreased from 391 to 299 MPa). Still, the ductility was approximately 200% (in-creased from 3.2 to 6.8%) higher than the as-built specimen. This is because spherical silicon particles become coarsened when the specimen ductility is increased after heat treatment. For fatigue behaviour, it shows the as-built and heat-treated specimens are closely similar compared to findings from the literature. Overall, this study showed that the post-process changed the tensile strength and microstructural of AlSi10Mg but only significantly improved fatigue performance.

Keywords AlSi10Mg · Additive manufacturing · DMLS · Fatigue life · Mechanical characterization

S. P. Tan · M. A. Ramlan · M. S. Shaari (✉) · M. R. M. Akramin
Faculty of Mechanical and Automotive Engineering Technology, Universiti Malaysia Pahang, 26600 Pekan, Pahang, Malaysia
e-mail: shamil@ump.edu.my

A. Takahashi
Department of Mechanical Engineering, Faculty of Science & Technology, Tokyo University of Science, 2641 Yamazaki, Noda-shi, Chiba-ken 278-8510, Japan

1 Introduction

Recently, AM has been further applied into the advanced manufacturing industries by producing end-products (final parts). Several additive manufacturing (AM) techniques and processes are widely used by giant and well-known manufacturing companies such as Boeing, BMW, GE, and many more. Therefore, expanding the AM technology key player and hitting the manufacturing markets worldwide is essential. The AM material also varies from different types of metals such as aluminum alloy or titanium and non-metallic such as nylon or polystyrene. Meanwhile, it is still limited to only a few types of materials. Findings that provide similar outcomes towards AM technique can be found in several studies done by researchers in the field, such as SS316L material [1], TiAl6V4 material [2], and AlSi10Mg material [3–5]. Proportionally, the process and technology driving the AM machinery also evolve hastily. It started from selective laser sintering (SLS) in the mid-1980s, followed by electron beam melting (EBM) in the early 1990s, selective laser melting (SLM), and direct metal laser sintering (DMLS) in the mid-1990s [6].

Despite meeting manufacturing efficiency, the integrity of AM must be further studied to ensure human safety indemnity in AM-produced components, especially for automotive, aerospace, and oil and gas industries. Thus, the static, dynamic and mechanical characteristic of AM has to be well explored and forecasted [7]. Fatigue ehavior of AM material is put into relation confrontation in between AM process [7], built orientation [8, 9], surface roughness and porosity [10, 11], the effect of post-processes [12] and mechanical properties [11]. Furthermore, microstructure analysis studies were carried out to understand the characteristics of AM material on changes after mechanical properties [13, 14]. According to [11], these components influence the mechanical properties particularly heat treatment and surface roughness emphatically affects the fatigue strength. Meanwhile, structural integrity analysis is applied to every AM produced component because cracks emerge from fatigue and fracture behavior when cycling stresses are applied [15–17].

Previous studies have a lack of research on the structural integrity of AM material. Also, most studies on AlSi10Mg material are commonly fabricated by the SLM method [18]. Most research on the DMLS method is still in the initial stage, not as mature as the SLM method. Therefore, the material characteristics and microstructure of AlSi10Mg fabricated by DMLS are investigated in this paper. The aim is to determine the integrity of AlSi10Mg material manufactured by the DMLS technique based on mechanical characterization. In the following, the response of post-treatment on AM material manufactured by DMLS is compared to the as-built model. Several types of experimental work on post-treatment are carried out. The changes in the material properties and fatigue strength affected by the post-process of AlSi10Mg are studied and discussed.

2   Methodology

The effect of post-process on the AM material is conducted in this paper. A flow chart of the methodology in this paper is shown in Fig. 1. First, a DMLS machine fabricated all experimental work specimens. Afterwards, specimens remained as-built (AB) condition and underwent different types of post-process. Several types of post-processes were carried out in this study which are annealing (TS), solution heat treatment (T6), and artificial ageing (T5 & T6) processes.

The preparation and fabrication of the AlSi10Mg samples using the DMLS can be divided into three stages, pre-process, laser sintering, and post-process. Before the product can be printed using the DMLS method, the input files for the components should be produced using the 3D computer-aided design (CAD) software. Next, the model is designed in CAD software before creating an output file known as a stereolithography (STL) file. This file will be the input file for the AM machine for fabrication purposes. The support structures are also included along with the model before the final slicing process is performed. The sliced file then is imported into the EOS M290 via a computer onboard with the machine.

After that, several specimens were further for post-process. Those specimens underwent the annealing process at 300 °C for 2 h before going through T5 and T6

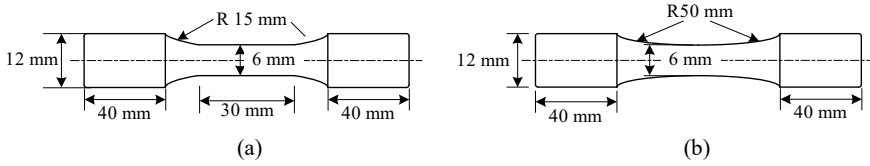**Fig. 1** Experimental workflow chart
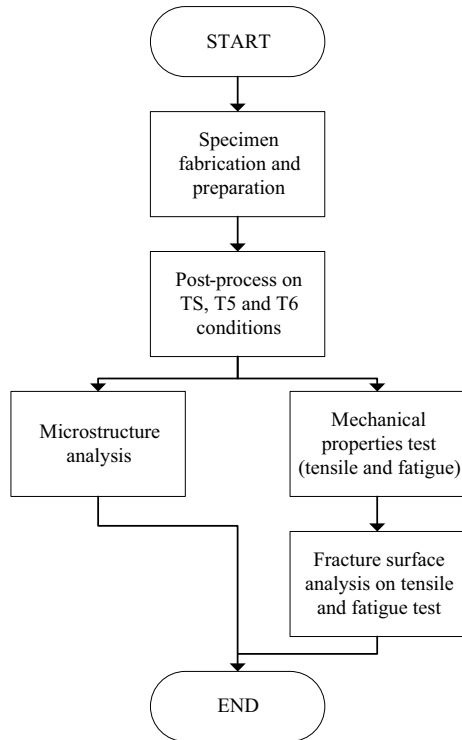
Fig. 2 Geometry design of samples for **a** tensile test **b** fatigue test

processes. For T6, 520 °C for 6 h was applied, then quenched with water at room temperature. Lastly, the temperature for artificial ageing is set at 165 °C, heated for 7 h before being removed, and cooled down at room temperature.

Two types of microstructure analysis were carried out namely scanning electron microscope (SEM) with energy dispersive spectroscopy (EDAX) and optical microscope. First, microstructure characterization was performed to study the microstructure on all specimens. Next, the tensile test is performed to determine the mechanical properties of AM material. This test was conducted by a universal tensile machine (UTM) following the American Society for Testing and Materials (ASTM) E8 standard. Then, an Instron testing machine conducted the fatigue test at room temperature. During the experiment, an ASTM E466 standard stress-controlled testing mode is applied. The test's overhead speed (1.8 mm/min) and strain rate (1×10^{-3} s^{-1}) are set. For cyclic loading, the test is based on a sinusoidal wave at 15 Hz frequency and a stress ratio of 0.1 (R = $\sigma_{min}/\sigma_{max}$). Then, the fracture surfaces of both tensile and fatigue samples are inspected and analyzed under an optical microscope.

Figure 2 is the geometry of samples used for the tensile test and fatigue test. These specimens are fabricated based on the respective ASTM standards. For example, Fig. 2a shows the geometry design for a tensile sample with a gauge length of 30 mm which is used in the tensile testing. On the other hand, Fig. 2b indicates the sample with a 50 mm continuous radius and a minimum of 6 mm diameter used in fatigue testing. Each specimen was built vertically to build a platform and manufactured using the EOS M290 machine. All samples are inspected for imperfection on the surface like sharp edges and any cracks before going through the test.

3 Results and Discussion

3.1 Microstructure of As-Built vs Heat Treated on AlSi10Mg

Figure 3 reveals the microstructure of the metallographic cross-sectioned of as-built AlSi10Mg specimens. It consists of α-Al columnar fine grains (dendrites) with Si-particles (interdendrites) disclosed at the melt pool and the boundaries. Figure 3a and b show clearly that the particles of as-built AlSi10Mg material have overlapped and segregated at melt pools and boundaries during laser sintering [19, 20]. According to Aboulkhair et al. [19], this kind of fine microstructure formation is because of
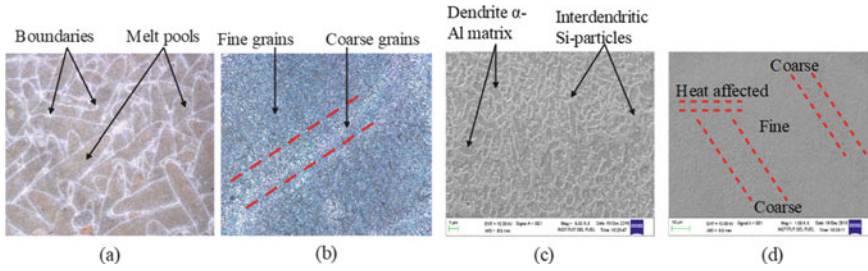
Fig. 3 Microstructure of AlSi10Mg for the as-built specimen. Under the microscope: **a** 500 μm. **b** 50 μm. Under SEM of the as-built specimen. **c** Magnification at 1 μm **d** Magnification at 10 μm

the rapid cooling rate during fabrication processing. The traces of a series of a laser beam that passes on the specimens create heat-affected zones with visible coarser particles, resulting in an inhomogeneous microstructure [20].

Figure 3c and d show the magnified image at the centre of the melt pool. A fine microstructure of cellular dendrites of α-Al and interdendrites of Si-are observed in the melt pool. Observed that, the grain size becomes coarser and segregated rather than spherical near the melt pool boundary. Keeping specimens at high temperatures with long hours caused the coarsening characteristic since overlapping two adjacent melt pools results in a slower solidification rate. The fine grains of the as-built AlSi10Mg specimens are attributed to the even arrangement of the Si particles in the microstructure of the specimen, which is likely due to the precipitation of the silicon phase along the Al-Si cellular boundaries.

Figures 4 are exhibit the microstructure for the heat-treated specimen which was conducted using SEM. The behaviour of microstructure is clearly displayed. Figure 4a and b show a microstructure with a columnar morphology indicating fine cellular-dendritic growth of Al matrix and interdendritic Si-particles during solidification. The grey cellular features are primarily Al particles and are surrounded by white fibrous Si particles. In contrast, Fig. 4c and d show the different areas in the melt pool. Thijs et al. [21] found that the microstructure of AlSi10Mg produced by the AM method is characterized by three regions across the melt pool: a fine and
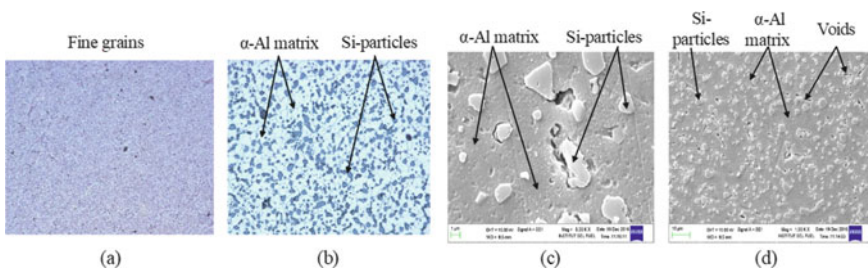

Fig. 4 Microstructure of AlSi10Mg for the heat-treated specimen. Under microscope: **a** 500 μm. **b** 50 μm. Under SEM of heat-treated (T6) SLM AlSi10Mg. **a** 1 μm. **b** 10 μm

a coarse cellular structure inside the melt pool heat-affected (transition) zone and around the melt pool in the previously deposited layers. In the transition zone, the eutectic Al-Si network structure is broken to some extent by coarsening the Si into spheroidized particles, which increases the diffusion rate of the Si [22]. The different thermal histories experienced by three regions have been attributed in contact with readily solidified Al. At the same time, the Al has less heat conductivity due to slower solidification [13, 23].

3.2 Tensile Test

Following are the tensile test results of as-built and post-process AlSi10Mg specimens that were carried out at room temperature as shown in Table 1 and Fig. 5. Based on the result, realized that the yield and tensile strength were reduced post-processed. Meanwhile, the ductility of the specimens after post-process was increased.

From the result, the specimens showed brittle behaviour when the strain was just above 3% under quasi-static loading. The AB specimens showed the highest tensile and yield strength of 391.0 MPa and 233.0 MPa respectively yet retained the

Table 1 Experimental tensile test results

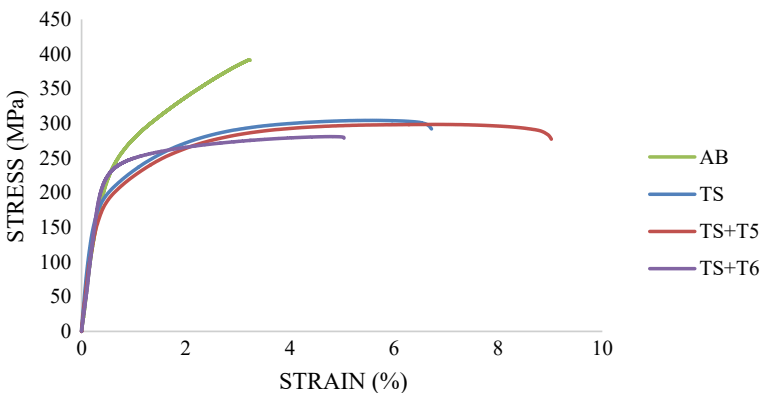| Specimens	Yield Strength, 0.2% offset (MPa)	Ultimate Tensile Strength (MPa)	Modulus of Elasticity (GPa)	Strain (%)
AB	233.0	391.0	62.0	3.2
TS	192.0	304.0	79.9	5.6
TS + T5	187.0	299.0	64.3	6.8
TS + T6	227.0	287.0	74.0	6.6

Fig. 5 Comparison of tensile results between as-built and post-processed for AlSi10Mg

lowest ductility of 3.2% in strain. The annealing process (TS) made an incredible impact on the mechanical properties. After the specimen went through the annealing process, great drop in yield strength and tensile strength (192.0 MPa and 304.0 MPa) was observed. However, the ductility is improved, and the strain increases by 5.6%. Meanwhile, the specimens experienced annealing with artificial aging on T5 and T6 condition also found a similar result. Both decreased tensile (at 299.0 MPa and 287.0 MPa) and dramatically increased ductility (at 6.8% and 6.6%), respectively. The annealed specimens have been softening compared to AB. The T6 specimen is the only sample that experienced the peak-hardened solution heat treatment (SHT) process. Even though the specimen has the lowest UTS among all specimens, the yield strength is as high as the AB specimen.

The AB specimen consists of high strength and can be a virtue to grain refinement. This is due to the mechanical properties affected by the grain size [24]. For the specimen after heat-treated, the strength and ductility changes are influenced by several factors such as the change of Si phases in terms of number or size, formation of Mg2Si, the initial hardening rate, recovery rate, etc. [25]. Upon the SHT and artificial ageing, the Si atom is trapped in the Al matrix, and the distance between Si–Si particles increases simultaneously. Meanwhile, the size of Si particles increased, which induced localized stress and strain reduction [26]. Based on the tensile test result, the ductile and brittleness of the material is difficult to categorize by heeding the number of strains only [27]. So, the fracture surface of the specimen investigation is conducted. Alboulkhair et al. [3] claimed that initial failure always starts at a surface or sub-surface imperfection then propagates along the plane opposite to the loading direction until the final crack.
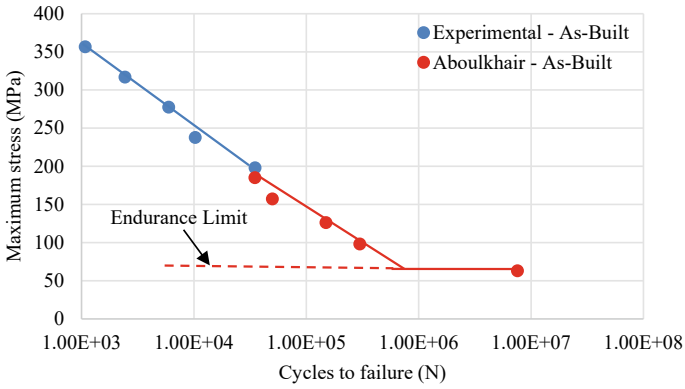
3.3 Fatigue Test

Results of data obtained from a series of fatigue experiments are plotted according to the stress-life (S–N) method. Table 2 and Table 3 both listed the overall fatigue test results for the as-built and heat-treated specimens respectively. Furthermore, the loading parameters used in fatigue testing are also included in the table. From the fatigue test, the stresses are different for as-built and heat-treated. The loading

**Table 2** Overall fatigue test results for as-built AlSi10Mg

Specimens	Cycles to Failure	σ_{max} (MPa)	σ_{min} (MPa)	σ_{mean} (MPa)
90% UTS	1.08×10^3	356.31	35.60	195.97
80% UTS	2.44×10^3	316.72	31.67	174.20
70% UTS	5.99×10^3	277.33	27.71	152.42
60% UTS	1.03×10^4	237.54	23.75	130.65
50% UTS	3.51×10^4	197.95	19.80	108.87

Table 3 Overall fatigue test results for heat-treated AlSi10Mg

Specimens	Cycles to Failure	σ_{max} (MPa)	σ_{min} (MPa)	σ_{mean} (MPa)
90% UTS	3.77×10^4	258.48	25.85	142.16
80% UTS	6.05×10^4	229.26	22.98	126.37
70% UTS	1.99×10^5	201.04	20.10	110.57
60% UTS	5.08×10^5	143.02	17.23	94.78
50% UTS	2.13×10^6	96.24	14.36	78.98

(a)
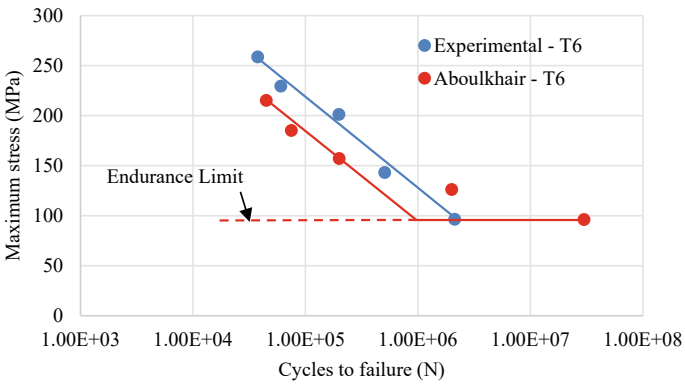
(b)

Fig. 6 Comparison of fatigue behavior between experimental and previous study for **a** as-built [3] and **b** heat-treated specimens

parameters are designed accruing to the UTS. Five specimens underwent fatigue testing for each case for the level of stress from 90 to 50% of the UTS.
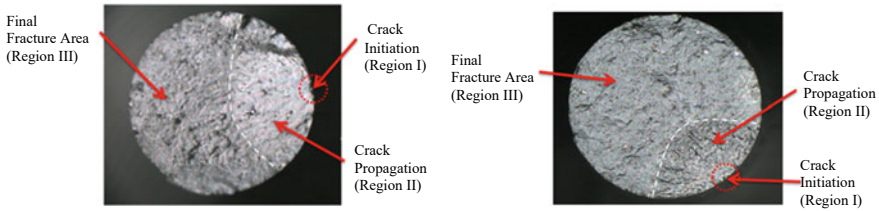
Fig. 7 Fatigue fracture surface of **a** as-built **b** T6

Figure 6 shows the fatigue behaviour of the specimens based on the fatigue data plotted. These data are plotted according to the stress-life (*S–N*) curve and compared to the results of the previous study. The fatigue life behaviour is comparable to the results from Aboulkhair et al. [3]. Since the level of stresses for as-built in the previous study is lower than the experiment, thus the cycles to failure are significantly lower than the experimental results for as-built. However, for the heat-treated, the level of stress is almost similar. Hence, the fatigue life result is better compared to the previous study. One of the reasons is the author performed SHT for T6 in a different way. The specimens only underwent heat treatment for 1 h at 520 °C before water quenched unlike this study; for 6 h. The microstructure is likely not having enough time for the Si to spheroidized. The formation of Si spheroids through spheroidization results in strengthening the material through the heat treatment process. On the other hand, an endurance limit was analyzed based on the *S–N* curve. The performance was increased significantly after heat-treated by T6 condition. In comparison to as-built specimen, heat-treated showed a similar number of cycles in all manner of stress ranges, favourable fatigue behaviour in low-stress range, and with no overrun during the test even performed at 96.24 MPa for maximum stress.

Figure 7 shows the crack propagation and fatigue fracture on the surface of the specimen after undergoing fatigue tests for as-built and heat-treated specimens. It is found that, the crack initiation is the result of defects in the material. The fracture surface is flat around the crack initiation part from a macroscopic appearance viewpoint and this is also found in the study of Mcmillan & Hertzberg [28].

The whole fatigue-fracture surface consisted of four main regions. There are (i) fatigue cracked region, (ii) stretched region, (iii) overload fracture region, and (iv) final fracture region. However, certain researchers considered the second and third regions as the fatigue crack propagation region [27]. In SLM, two types of crack initiation under fatigue loading are categorized [29]. The first type is planar fabrication flaws such as lack of penetration or fusion provide ideal sites for fatigue cracking. The second type is failure due to poor surface roughness during the fabrication of the specimens. The effect of post-process on crack propagation and fatigue fracture inside the test specimen is indicated in Fig. 7b. It is observed that the heat-treated specimen is reasonably flat and uniform on the fracture surface. However, some tiny dimples appear on the fracture surface, and it is restricts the perception of the specimen with any process. It is moreover evident that the heat treatment caused the microstructural coarsening.

4   Conclusions

In this paper, both the microstructure and mechanical properties of AlSi10Mg alloy on as-built and post-process were studied. The main conclusions are the following:

- The microstructure is made up of melt pools with boundaris, while the core of the melt pool is fine and uniform in grain structure. After post-process, spheroidization of Si particles was formed and coarsened.
- For the mechanical properties of this alloy after several types of post-process, it is appealing to increase ductility yet decrease in tensile strength. The as-built consists of the highest tensile strength (391 MPa) but lowest ductility (3.2%) among all specimens. Meanwhile, the T5 thermal processed specimen annealed has the highest ductility (6.8%) but lower tensile strength (299 MPa). This is due to the spheroidization of Si particles observed in the microstructure.
- As observed, when a different SHT approach is applied, heat-treated specimen's cycles to failure have significantly enhanced fatigue life compared to as-built in comparison to the previous study.

Further studies need to be performed to understand fatigue crack behaviour and propagation of the specimens. This is mainly for studies on the different types of specimens with different types of post-process when without annealing. This is important to understand the structural integrity performance of material applied to different applications.

References

1. Duval-Chaneac MS, Gao N, Khan RHU, Giles M, Georgilas K, Zhao X, Reed PAS (2021) Fatigue crack growth in IN718/316L multi-materials layered structures fabricated by laser powder bed fusion. Int J Fatigue 152:106454
2. Lee S, Ahmadi Z, Pegues JW, Mahjouri-Samani M, Shamsaei N (2021) Laser polishing for improving fatigue performance of additive manufactured Ti-6Al-4V parts. Opt Laser Technol 134:106639
3. Aboulkhair NT, Maskery I, Tuck C, Ashcroft I, Everitt NM (2016) Improving the fatigue behaviour of a selectively laser melted aluminium alloy: influence of heat treatment and surface quality. Mater Des 104:174–182
4. Ch SR, Raja A, Jayaganthan R, Vasa NJ, Raghunandan M (2020) Study on the fatigue behaviour of selective laser melted AlSi10Mg alloy. Mater Sci Eng, A 781:139180
5. Xu Z, Liu A, Wang X (2021) Fatigue performance and crack propagation behavior of selective laser melted AlSi10Mg in 0°, 15°, 45° and 90° building directions. Mater Sci Eng, A 812:141141

6. Venuvinod PK, Ma W (2004) Rapid prototyping: laser-based and other technologies. Springer Science + Business Media, New York

7. Ferro P, Fabrizi A, Berto F, Savio G, Meneghello R, Rosso S (2020) Defects as a root cause of fatigue weakening of additively manufactured AlSi10Mg components. Theoret Appl Fract Mech 108:102611

8. Tridello A, Fiocchi J, Biffi CA, Chiandussi G, Rossetto M, Tuissi A, Paolino DS (2020) Effect of microstructure, residual stresses and building orientation on the fatigue response up to 109 cycles of an SLM AlSi10Mg alloy. Int J Fatigue 137:105659

9. Beretta S, Gargourimotlagh M, Foletti S, du Plessis A, Riccio M (2020) Fatigue strength assessment of "as built" AlSi10Mg manufactured by SLM with different build orientations. Int J Fatigue 139:105737

10. Leon A, Aghion E (2017) Effect of surface roughness on corrosion fatigue performance of AlSi10Mg alloy produced by Selective Laser Melting (SLM). Mater Charact 131:188–194

11. Beevers E, Brandão AD, Gumpinger J, Gschweitl M, Seyfert C, Hofbauer P, Rohr T, Ghidini T (2018) Fatigue properties and material characteristics of additively manufactured AlSi10Mg— effect of the contour parameter on the microstructure, density, residual stress, roughness and mechanical properties. Int J Fatigue 117:148–162

12. Bagherifard S, Beretta N, Monti S, Riccio M, Bandini M, Guagliano M (2018) On the fatigue strength enhancement of additive manufactured AlSi10Mg parts by mechanical and thermal post-processing. Mater Des 145:28–41

13. Fite J, Eswarappa Prameela S, Slotwinski JA, Weihs TP (2020) Evolution of the microstructure and mechanical properties of additively manufactured AlSi10Mg during room temperature holds and low temperature aging. Addit Manuf 36:101429

14. Varmus T, Konecna R, Nicoletto G (2021) Microstructure and fatigue performace of additively manufactured AlSi10Mg. Transp Res Procedia 55:518–525

15. Akramin MRM, Shaari MS, Ariffin AK, Kikuchi M, Abdullah S (2015) Surface crack analysis under cyclic loads using probabilistic S-version finite element model. J Braz Soc Mech Sci Eng 2015 37:6 37(6):1851–1865

16. Shaari MS, Akramin MRM, Ariffin AK, Abdullah S, Kikuchi M (2016) Prediction of fatigue crack growth for semi-elliptical surface cracks using S-version fem under tension loading. J Mech Eng Sci (JMES) ISSN 10(3):2375–2386

17. Zhang W, Hu Y, Ma X, Qian G, Zhang J, Yang Z, Berto F (2021) Very-high-cycle fatigue behavior of AlSi10Mg manufactured by selected laser melting: crystal plasticity modeling. Int J Fatigue 145:106109

18. Jian ZM, Qian GA, Paolino DS, Tridello A, Berto F, Hong YS (2021) Crack initiation behavior and fatigue performance up to very-high-cycle regime of AlSi10Mg fabricated by selective laser melting with two powder sizes. Int J Fatigue 143:106013

19. Aboulkhair NT, Maskery I, Tuck C, Ashcroft I, Everitt NM (2016) The microstructure and mechanical properties of selectively laser melted AlSi10Mg: the effect of a conventional T6-like heat treatment. Mater Sci Eng, A 667:139–146

20. Zhou L, Mehta A, Schulz E, McWilliams B, Cho K, Sohn Y (2018) Microstructure, precipitates and hardness of selectively laser melted AlSi10Mg alloy before and after heat treatment. Mater Charact 143:5–17

21. Thijs L, Kempen K, Kruth JP, Van Humbeeck J (2013) Fine-structured aluminium products with controllable texture by selective laser melting of pre-alloyed AlSi10Mg powder. Acta Mater 61(5):1809–1819

22. Zhuo L, Wang Z, Zhang H, Yin E, Wang Y, Xu T, Li C (2019) Effect of post-process heat treatment on microstructure and properties of selective laser melted AlSi10Mg alloy. Mater Lett 234:196–200

23. Aboulkhair NT, Everitt NM, Ashcroft I, Tuck C (2014) Reducing porosity in AlSi10Mg parts processed by selective laser melting. Addit Manuf 1–4:77–86

24. Li W, Li S, Liu J, Zhang A, Zhou Y, Wei Q, Yan C, Shi Y (2016) Effect of heat treatment on AlSi10Mg alloy fabricated by selective laser melting: microstructure evolution, mechanical properties and fracture mechanism. Mater Sci Eng, A 663:116–125

25. Hadadzadeh A, Amirkhiz BS, Mohammadi M (2019) Contribution of Mg2Si precipitates to the strength of direct metal laser sintered AlSi10Mg. Mater Sci Eng, A 739:295–300
26. Li XP, Wang XJ, Saunders M, Suvorova A, Zhang LC, Liu YJ, Fang MH, Huang ZH, Sercombe TB (2015) A selective laser melting and solution heat treatment refined Al-12Si alloy with a controllable ultrafine eutectic microstructure and 25% tensile ductility. Acta Mater 95:74–82
27. Brooks CR, Choudhury A (2002) Failure analysis of engineering materials. McGraw-Hill Education, New York
28. McMillan JC, Hertzberg RW (1968) Application of electron fractography to fatigue studies. Electron Fractography 89–123
29. Wycisk E, Solbach A, Siddique S, Herzog D, Walther F, Emmelmann C (2014) Effects of defects in laser additive manufactured Ti-6Al-4V on fatigue properties. Phys Procedia 56(C):371–378